

PAPER • OPEN ACCESS

# CMOS charge qubits and qudits: entanglement entropy and mutual information as an optimization method to construct CNOT and SWAP Gates

To cite this article: Panagiotis Giounanlis *et al* 2021 *Semicond. Sci. Technol.* **36** 095014

View the [article online](#) for updates and enhancements.



## You may also like

- [An optimization method of acceleration and deceleration time of feed system based on load inertia](#)  
Hao Zhou, Jianzhong Yang, Yongjie Guo et al.
- [One decade of quantum optimal control in the chopped random basis](#)  
Matthias M Müller, Ressa S Said, Fedor Jelezko et al.
- [Self sustained thermally induced gas-damped oscillations of bimetal cantilevers with application to the design of a new pyroelectric micro energy harvester](#)  
Tarek Gebrael, Ali Kanj, Daniel Farhat et al.

**ECS**  
The  
Electrochemical  
Society  
Advancing solid state &  
electrochemical science & technology

**DISCOVER**  
how sustainability  
intersects with  
electrochemistry & solid  
state science research

# CMOS charge qubits and qudits: entanglement entropy and mutual information as an optimization method to construct CNOT and SWAP Gates

Panagiotis Giounanlis<sup>1,\*</sup> , Xutong Wu<sup>1,2</sup>, Andrii Sokolov<sup>1,2</sup>, Nikolaos Petropoulos<sup>1,2</sup>, Eugene Koskin<sup>2</sup>, Imran Bashir<sup>3</sup>, Dirk Leipold<sup>3</sup>, Robert Bogdan Staszewski<sup>1,2</sup> , and Elena Blokhina<sup>1,2,\*</sup>

<sup>1</sup> Equal1 Laboratories, NovaUCD, Belfield, Dublin 4, Ireland

<sup>2</sup> University College Dublin, Belfield, Dublin 4, Ireland

<sup>3</sup> Equal1 Laboratories, Fremont, CA 94536, United States of America

E-mail: [panagiotis.giounanlis@equal1.com](mailto:panagiotis.giounanlis@equal1.com), [elena.blokhina@ucd.ie](mailto:elena.blokhina@ucd.ie) and [elena.blokhina@equal1.com](mailto:elena.blokhina@equal1.com)

Received 4 December 2020, revised 11 January 2021

Accepted for publication 11 February 2021

Published 30 July 2021



## Abstract

In this paper, we propose an optimization method for the construction of two-qubit and two-qudit quantum gates based on semiconductor position-based charge qubits. To describe the evolution of various quantum states, we use a Hubbard based model and Lindblad formalism. The suggested optimization algorithm uses the time evolution of entanglement entropy and mutual information for the determination of the system parameters to achieve high fidelity gates.

Keywords: charge qubits, CMOS technology, entanglement entropy, tight binding formalism, qudits, quantum gates

(Some figures may appear in color only in the online journal)

## 1. Introduction

Semiconductor quantum devices are becoming promising candidates for the implementation of quantum computation due to their potential of large-scale integration. Several quantum technology architectures have been proposed for semiconductor based qubits, involving the manipulation of spin, spin-orbit, or charge degrees of freedom [1–4]. Although single-qubit and two-qubit gates have been reported in the literature [5–10], the construction of CNOT and SWAP quantum gates with high fidelity is still a challenging issue.

One- and two-qubit gates have been constructed for semiconductor spin or hybrid qubits [2, 7, 8, 11, 12], or even through laser pulse-assisted quantum logic [13]. Single-qubit gates have been demonstrated for charge qubits [14]. There are some attempts in the literature presenting two-charge-qubit gates, for example by the conditional rotation of two coupled quantum dots [15], or even through the manipulation of a four-level system [5]. Moreover, various approaches to enhance the fidelity of quantum gates due to decoherence effects, noise, and other uncertainties have been proposed, including feedback control methods [16], quantum optimal control based pulse generation [17], learning pulse sampling techniques [18], deep reinforcement learning [19], and others. However, these studies were mainly to obtain the desired amplitudes of the various quantum states through analytical approaches without taking into account the non-diagonal terms of the density matrix. They also do not extend to the cases of multiple system parameters and more complex

\* Authors to whom any correspondence should be addressed.



Original Content from this work may be used under the terms of the [Creative Commons Attribution 4.0 licence](https://creativecommons.org/licenses/by/4.0/). Any further distribution of this work must maintain attribution to the author(s) and the title of the work, journal citation and DOI.

geometries different than the conventional two-qubit ones. Therefore, the construction of two or multiple charge qubit gates with high fidelity is an open issue. In addition, some of these studies and proposed algorithms refer to an abstract Hamiltonian and do not connect the methodology with the actual technology and specific geometry of the charge-based qubits.

In this study, we demonstrate an optimization algorithm to achieve high fidelity two-qubit and two-qudit gates (CNOT, SWAP) through the example of a quantum core based on 22-nm fully depleted silicon-on-insulator (FD-SOI) devices [20, 21]. For this purpose, we introduce for the first time the Von Neumann entanglement entropy (EE) as an optimization tool. However, since EE cannot be measured directly, we also connect the process of finding the desired system parameters through the simulated measurement data with the use of mutual information (MI), and variance (Var) of the various random variables and their distributions as would be seen from the system detectors. Although the optimization process has been performed for charge qubits/qudits and refers to a particular structure/technology, the methodology followed in the current work applies to any kind of qubits/qudits. In addition, one cannot avoid a discussion on the decoherence of charge qubits since it has been always seen as their bottleneck. With several publications arguing that the charge qubits can stay coherent long enough if their geometry and operation frequencies are optimized [22–24], we have a dedicated discussion on the effect of decoherence, taking some realistic dephasing times as an example. Finally, we should mention that for the purpose of simulations in this study, a simulation backend for charge qubits compatible with IBM's Qiskit has been developed.

The paper is organized as follows. In section 2, we introduce the system under study which consists of a quantum core based on FD-SOI devices. In section 3, we discuss a Hubbard based model to describe the evolution of various quantum states in the system. We also review single-electron rotation quantum gates including, in the general case, decoherence, by the use of Lindblad equation [25, 26]. Finally, in section 5, we investigate the construction of two-qubit/qudit quantum gates, CNOT and SWAP, where with the use of EE we implement an optimization algorithm to find the required system parameters to achieve high fidelity.

## 2. Hardware implementation of charge qubits in FD-SOI technology

The system under study is based on a double V-shape geometry of quantum dot arrays (QDA) built in the 22-nm FD-SOI node of CMOS technology from GlobalFoundries as presented in [20, 21].

In the quantum dot array, which consists of several quantum dots (QD), particles (electrons) can be confined in the 5 nm thin silicon channel restricted by a potential energy profile manipulated by electrostatic control utilizing valid voltage pulses at the imposers/gates (see figure 1). The figure shows the principal structure of a quantum dot array. For simulations, a 3D structure that takes into account the technology

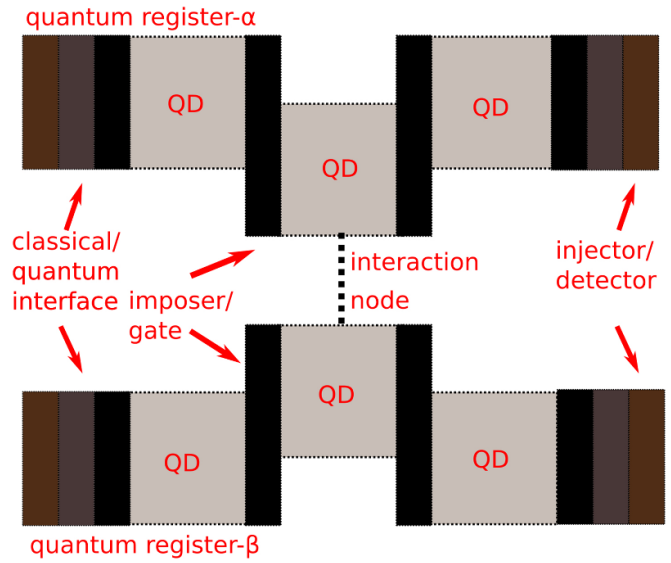


**Figure 1.** V-shape geometry realized in 22-nm FD-SOI technology [20]. The system consists of two quantum registers. Each quantum register includes three QDs and two single-electron detector/injector devices at the edges. The interaction node is where the electrostatic interaction between the two quantum registers would be maximum.

layers and is faithful to the devices reported in the literature is developed [27, 28]. The detailed view of the model, its cross-section, and the potential energy developed in the structure as a response to typically applied voltages are illustrated in figure 2. One can see the formation of 2D quantum wells with a depth of a few to tens of meV. The potential energy is simulated using the layout of the structure in COMSOL Multiphysics.

Interface single-electron (SET) devices at the edges of the structure serve as injectors/detectors. An injector is a device that can inject an electron (or a controllable small number of electrons) into the quantum core, whilst a detector device can detect the presence of a particle (or more) during the measurement procedure. The time evolution of the probabilities of various quantum states can be controlled by the gates (imposers) across the quantum register, which consists of a series of QDs forming a QDA. To construct quantum gates in such a structure, one needs to precisely control the potential barrier(s) which separate the adjoined QDs. This changes the tunneling probabilities of the particles. As a result, one can modulate the wavefunction which describes the system to facilitate quantum logic. Notice that the geometry of this system includes the interaction node, where the Coulomb force between neighboring particles of different quantum registers can be maximum.

## 3. Multi-quantum-dot register model in the second quantisation formalism

In [4], we solved the Schrödinger equation for a system of multiple quantum dots of multiple energy levels, and we demonstrated how one can associate the effective mass and the wave-function of the particle(s) with the parameters of the tight-binding model. In the present study, we will use a model

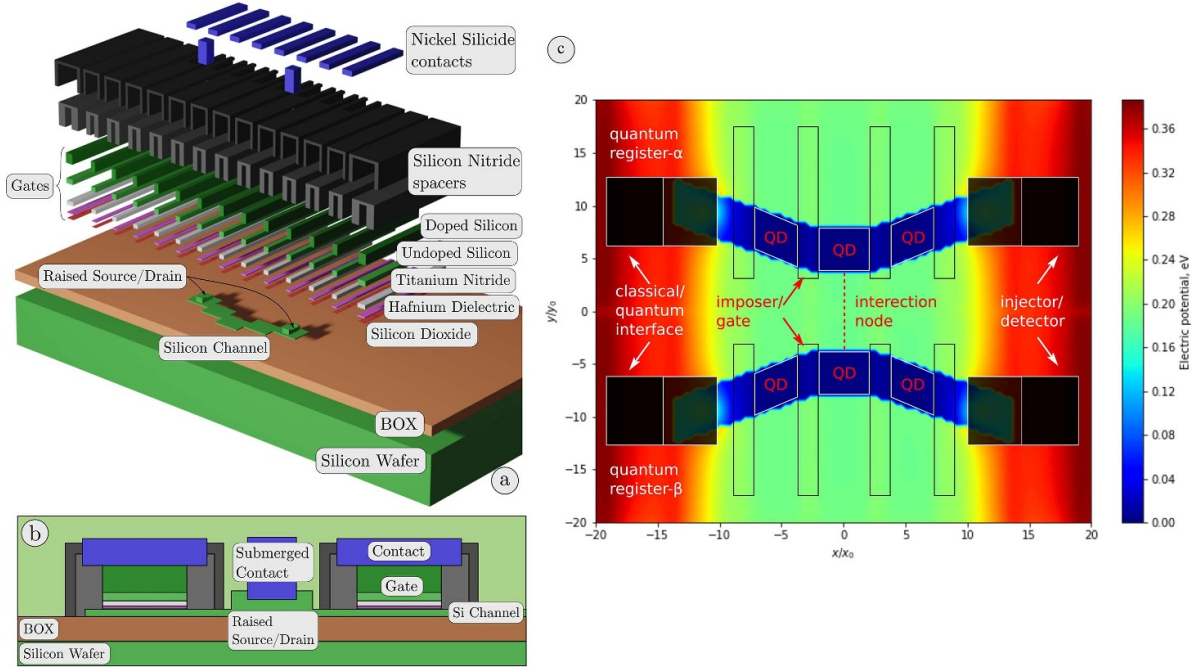


**Figure 2.** (a) Finite-element multi-layer model of a 22-nm FD-SOI device used in this study. (b) Cross-section of one of the devices of the V-shape quantum-dot arrays. (c) Potential energy and formation of 2D quantum wells in the regions between imposers in the V-shape structure consisting of multiple QDs. The depth of the quantum well is defined by the built-in E-field due to the semiconductor structure and the electric potential applied at the imposers.

expressed in terms of second quantisation with its parameters associated with 22-nm FD-SOI devices. Using two V-shape lines as an example, we can visualize the presented quantum structures as a pseudo-2D lattice of interacting QDs. In second quantisation, the state of the system is represented by the occupation number vector

$$|n\rangle = |n_1 \ n_2 \ \dots, m_1 \ m_2 \ \dots\rangle \quad (1)$$

where the occupation number  $n_j$  represents the occupation of the  $j$ th dot in the upper line and the occupation number  $m_j$  represents the occupation of the  $j$ th dot in the lower line. In the fermionic case,  $n_j = \{0, 1\}$  and  $m_j = \{0, 1\}$ . Each occupation number  $n_j$  is associated with the creation and annihilation operators  $\hat{c}_{1,j}^\dagger$  and  $\hat{c}_{1,j}$  so that  $\hat{n}_{1,j} = \hat{c}_{1,j}^\dagger \hat{c}_{1,j}$  is the occupation number operator for the  $j$ th dot in the upper line. Similarly, the excitation operator  $\hat{c}_{1,j+1}^\dagger \hat{c}_{1,j}$  that removes an electron from the  $j$ th dot in the upper line and places it in the  $(j+1)$  dot in the upper line without affecting the lower line can be introduced. The operator  $\hat{c}_{2,j+1}^\dagger \hat{c}_{2,j}$  acts on an electron in the lower line, without affecting the upper line. Hence, these operators will be denoted as  $\hat{c}_{i,j}^\dagger$  and  $\hat{c}_{i,j}$ , where  $i = 1, 2$  and  $j = \{1, \dots, N\}$  with  $N$  representing the total number of dots in each line. This labeling approach can be easily extended to an arbitrary number of V-shape lines  $M$ , so we can conventionally assume that  $i = \{1, \dots, M\}$ .

Keeping this notation agreement in mind, the Hamiltonian of the system is written in the following form [3, 29, 30]

$$H = H_0 + H_t + H_v \quad (2)$$

where

$$H_0 = \sum_{i=1}^M \sum_{j=1}^N \epsilon_{i,j} \hat{c}_{i,j}^\dagger \hat{c}_{i,j} \quad (3)$$

is the on-site energy of each dot and

$$H_t = - \sum_{i=1}^M \sum_{j=1}^{N-1} \left( t_{i,jj+1} \hat{c}_{i,j+1}^\dagger \hat{c}_{i,j} + t_{i,j+1j}^* \hat{c}_{i,j}^\dagger \hat{c}_{i,j+1} \right) \quad (4)$$

accounts for tunneling (hopping) between neighbor dots with  $t_{i,jj+1}$  describing the tunneling probability between the dots with indices  $j+1$  and  $j$  in the  $i$ th line. We neglect the probability of a particle hopping to a distant QD since the wavefunction of a localized state in a QD decays exponentially with distance. We also implicitly neglect such configurations that two or more electrons can occupy the same dot (spinless electrons).

Conventionally, single-particle operators in the second quantisation formalism can be expressed through single-electron wavefunctions or orbitals  $\phi_k^{(i)}(\mathbf{r})$  in position space through the following integrals [29],

$$\begin{aligned} \epsilon_{i,j} &= \int d\mathbf{r} \phi_j^{(i)*}(\mathbf{r}) \left[ \frac{1}{2m^*} \hat{\mathbf{p}}^2 + V_p(\mathbf{r}) \right] \phi_j^{(i)}(\mathbf{r}) \\ t_{i,jj+1} &= \int d\mathbf{r} \phi_{j+1}^{(i)*}(\mathbf{r}) \left[ \frac{1}{2m^*} \hat{\mathbf{p}}^2 + V_p(\mathbf{r}) \right] \phi_j^{(i)}(\mathbf{r}). \end{aligned} \quad (5)$$



The third term in equation (2) represents the Coulomb interaction that is a two-electron operator:

$$H_U = \sum_{j=1}^M \sum_{k=1}^M \sum_{l=1}^N \sum_{m=1}^N U_{jk,lm} \hat{c}_{j,l}^\dagger \hat{c}_{k,m}^\dagger \hat{c}_{j,l} \hat{c}_{k,m} \quad (6)$$

where the prefactor  $U_{jk,lm}$  is a two-electron Coulomb integral between different quantum dot wavefunctions  $\phi(\mathbf{r})$ , given by:

$$U_{jk,lm} = \iint d\mathbf{r} d\mathbf{r}' \phi_l^{(j)*}(\mathbf{r}) \phi_m^{(k)*}(\mathbf{r}') \frac{e^2}{4\pi\epsilon_{r0} |\mathbf{r} - \mathbf{r}'|} \times \phi_l^{(j)}(\mathbf{r}) \phi_m^{(k)}(\mathbf{r}'). \quad (7)$$

Since we allow again only the nearest-neighbor Coulomb interaction, the non-zero terms will have indices  $m = l \pm 1$ . Therefore, for example, the term  $U_{jj,l+1}$  would correspond to the interaction integral of the  $l$ th dot electron with the one on the  $(l+1)$  dot, both residing on the  $j$ th line. Equations (5)–(7) relate the parameters of the tight-binding model to the microscopic wave-functions. The interested reader can refer to [4, 31] for a calculation of these parameters, wave-functions, and a relevant discussion.

In the case where the externally applied fields are constant in time, the Hamiltonian of the system can be assumed time-independent. In practice, this can happen when one applies a constant voltage to the imposers. In this work, we are also interested in describing the dynamics of the system for a time-dependent case, where the hopping coefficients  $t_{ij}$  do not remain constant with time. To perform quantum operations, one needs to apply a correct sequence of voltage pulses at the imposers (control gates) at specific time instances, changing the tunneling probabilities. In such a case, the Hamiltonian of the system is changing with time. In the system under study, an applied pulse causes a ‘sudden’ change in the Hamiltonian [32]. Also, the applied external fields (voltage pulses) will be assumed to have small magnitudes. We will also assume that the driving field is in resonance with the internal occupancy frequency between the eigenstates, thus the Rabi frequency between two quantum dots will be proportional to the tunneling probability [33].

The time evolution of the system can then be described from the Lindblad equation [34, 35]

$$\dot{\rho} = -\frac{i}{\hbar} [H, \rho] + \sum_{i=1}^{N^2-1} \Gamma_i \left( L_i \rho L_i^\dagger - \frac{1}{2} \{ L_i^\dagger L_i, \rho \} \right) \quad (8)$$

where  $\rho$  is the density matrix describing the quantum states of the system,  $L_i = u_{i,j} A_j$  are the jump operators, with  $u_{i,j}$  representing a unitary matrix, and  $A_j$  is an arbitrary orthonormal basis. Furthermore,  $\Gamma_i = \Gamma_{1i} + \Gamma_{2i}$  includes the spontaneous emission rate  $\Gamma_{1i}$ , and the pure dephasing rate  $\Gamma_{2i}$ .

### 3.1. Single-electron charge qubit representation

We start our analysis by considering the two-level system, consisting of two quantum dots. From (2) the Hamiltonian, in this case can be expressed as:

$$H(t) = \begin{pmatrix} |0\rangle & |1\rangle \\ \langle 0| & \langle 1| \end{pmatrix} \begin{pmatrix} E(t) + \Delta(t)/2 & t_{h,10}(t) \\ t_{h,10}^*(t) & E(t) - \Delta(t)/2 \end{pmatrix} \\ = E(t) \mathbf{I} + \frac{\Delta(t)}{2} \hat{\sigma}_z + \tau_{h,10}(t) \hat{\sigma}_x + \alpha_{h,10}(t) \hat{\sigma}_y \quad (9)$$

where the tunneling (hopping) terms  $t_{h,ij}(t) = \tau_{h,ij}(t) - i\alpha_{h,ij}(t)$  with  $h = 1, 2$  being the line index,  $i, j = 0, 1$  with  $i \neq j$  correspond to the qubit state and  $\tau_{h,ij}(t)$ ,  $\alpha_{h,ij}(t) \in \mathbb{R}$  the two elements which parametrize  $\hat{x}$  and  $\hat{y}$  axis rotations.

Tunneling can be modulated by a (time-dependent) manipulation of the separating potential energy barrier between two adjoined quantum dots (e.g. by applying voltage pulses on the imposer(s)).  $\Delta(t) = \epsilon_1(t) - \epsilon_0(t)$  is the relative potential energy difference between the QDs and can be modulated by the manipulation of their relative potential energy bottoms [4].  $E(t)$  is a global phase and can be removed from the Hamiltonian by a relevant phase transform since is not an observable. Finally, we should mention that the imaginary part of the hopping term,  $\alpha_{h,ij}(t)$  is associated with spin-orbit interaction in the presence of strong magnetic fields. In this work though, we will ignore the spin degrees of freedom; however, we include the imaginary term in the above expression for completeness.

### 3.2. Bloch sphere representation

A single electron in a double quantum dot (DQD) can represent a position-based charge qubit:

$$|\psi\rangle = c_0 |0\rangle + c_1 |1\rangle \equiv \cos\left(\frac{\theta}{2}\right) |0\rangle + e^{i\varphi} \sin\left(\frac{\theta}{2}\right) |1\rangle \quad (10)$$

where  $|c_0|^2 + |c_1|^2 = 1$ , and the angles  $\varphi \in [0, 2\pi)$  and  $\theta \in [0, \pi]$  define its Bloch sphere representation. The modulation of  $\theta(t)$  and  $\varphi(t)$  can be achieved by applying appropriate electrostatic actuation at the gate(s) or the well-bottoms of the structure.

The height of the middle barrier controls the frequency of these oscillations, i.e.  $\varphi \sim \omega_0 t$ , where  $\omega_0$  is the occupancy oscillation frequency [4]:

$$\cos^2\left(\frac{\theta}{2}\right) = \frac{1}{2} + |c_0||c_1| \cos(\omega_0 t) \\ \sin^2\left(\frac{\theta}{2}\right) = \frac{1}{2} - |c_0||c_1| \cos(\omega_0 t) \\ \varphi = \arctan\left[\frac{2|c_0||c_1| \sin(\omega_0 t)}{|c_0|^2 - |c_1|^2}\right]. \quad (11)$$

An extension to quantum registers consisting of a higher number of QDs and qudits is straightforward, as already discussed in [4].

### 3.3. One-qubit rotation gates

The one-qubit rotation gates can be implemented by applying a valid propagator to an initial qubit state:

$$|\psi_{t=T_G}\rangle = \mathbf{U}(T_G)|\psi_0\rangle \quad (12)$$

where  $T_G$  is the characteristic time that is needed for the actualization of an arbitrary gate application and depends on the system parameters, and

$$\mathbf{U}(t) = e^{-(i/\hbar) \int \mathbf{H}(\tau) d\tau} \quad (13)$$

is the propagator of the system. The time evolution expressed by (13), in the case of a time-dependent non-commuting Hamiltonian, can be calculated numerically by the use of Dyson series. By combining (9) and (13)

$$\begin{aligned} \mathbf{U}(t) &= e^{-(i/\hbar)[E\sigma_z + \tau\sigma_x + \alpha\sigma_y]t} \\ &= \lim_{n \rightarrow \infty} \left( e^{-(i/\hbar)E\sigma_z t/n} e^{-(i/\hbar)\tau\sigma_x t/n} e^{-(i/\hbar)\alpha\sigma_y t/n} \right)^n \end{aligned}$$

where the Lie product formula is applied. Here

$$\sigma_x = \begin{pmatrix} 0 & 1 \\ 1 & 0 \end{pmatrix}, \quad \sigma_y = \begin{pmatrix} 0 & -i \\ i & 0 \end{pmatrix}, \quad \sigma_z = \begin{pmatrix} 1 & 0 \\ 0 & -1 \end{pmatrix} \quad (14)$$

are the Pauli matrices which correspond to the rotation operations:

$$\begin{aligned} R_x(\theta_x) &= \begin{pmatrix} \cos \frac{\theta_x}{2} & -i \sin \frac{\theta_x}{2} \\ -i \sin \frac{\theta_x}{2} & \cos \frac{\theta_x}{2} \end{pmatrix}, \\ R_y(\theta_y) &= \begin{pmatrix} \cos \frac{\theta_y}{2} & -\sin \frac{\theta_y}{2} \\ \sin \frac{\theta_y}{2} & \cos \frac{\theta_y}{2} \end{pmatrix}, \quad R_z(\theta_z) = \begin{pmatrix} e^{-i\frac{\theta_z}{2}} & 0 \\ 0 & e^{i\frac{\theta_z}{2}} \end{pmatrix} \end{aligned} \quad (15)$$

where  $\theta_x, \theta_y, \theta_z$  are the corresponding rotation angles on the Cartesian coordinate system.

## 4. Results

In figure 3, the simulations of single-qubit quantum rotation gates are visualized. We compare the results obtained from (8), for the ideal case ( $\Gamma = 0$ ) with the ones obtained by the use of a numerical method which solves straightforwardly the time-dependent Schrödinger equation [31].

In equilibrium, the system in the eigenfunction representation is characterized by a fixed angle  $\theta$  with angle  $\varphi$  precessing at the frequency of occupancy oscillations  $\delta\omega = (E_1 - E_0)/\hbar$ , where the energy levels  $E_0$  and  $E_1$  are associated with the corresponding eigenstates  $|\psi_0\rangle$  and  $|\psi_1\rangle$ . Angle  $\theta$  can be adjusted by dynamically modulating the potential energy barrier between the neighboring QDs or by adjusting the bottoms of their potentials [4]. The used parameters are given in the table 1.

## 5. Two-qubit and two-qudit gates: using entanglement entropy as optimization tool through the example of a CNOT and a SWAP gate for charge qubits

In this section, we investigate the construction of quantum gates for a system of two qubits (where the unit of quantum logic is defined utilizing two QDs) and two qutrits (where the unit of quantum logic is defined utilizing three QDs) through the case study of a system of two charge qudits interacting via Coulomb force. Since the two qudits are assumed to be interacting and entangled, the evolution of the probability of quantum states of the system is non-linear. Therefore, after allowing the system to evolve for a specific time duration, and a given set of system parameters and geometry of the physical structure associated with the qudit technology/implementation, the output will depend on the initial conditions. However, two-qudit gates, with CNOT and SWAP quantum gates as an example, should be agnostic to the initial conditions. Consequently, one needs to optimize the time of operation of a two-qudit quantum gate for an arbitrary set of system parameters. For this purpose, we shall use the measure of entanglement entropy, as it is defined between the two interacting qudits, to optimize the timing of the operation, and an iteration algorithm for the overall optimization of the various parameters. In particular, for the charge qudit implementation, these parameters can be tuned by applying appropriate voltage pulses at the imposers/gates.

In the case of two interacting qubits via Coulomb force, the Hamiltonian of the system can be written as:

$$H = \begin{bmatrix} \Delta_{00} & t_{h,01,\beta} & t_{h,01,\alpha} & 0 \\ t_{h,10,\beta} & \Delta_{01} & 0 & t_{h,01,\alpha} \\ t_{h,10,\alpha} & 0 & \Delta_{10} & t_{h,01,\beta} \\ 0 & t_{h,10,\alpha} & t_{h,01,\beta} & \Delta_{11} \end{bmatrix} \quad (16)$$

where the diagonal terms, in this case, include the local potential energy and Coulomb interaction. They are statically set by the system geometry and can be dynamically modulated via the imposer voltages.

### 5.1. Definition of entanglement entropy and mutual information

Let us now consider the case of two qubits interacting via Coulomb repulsion and denoted as qubit #1 (system-*a*) and qubit #2 (system-*b*). In such a case, the particles' wavefunctions do not overlap each other since they are restricted in their respective region of the DQD. The combined wavefunction of this system can be expressed as:

$$\begin{aligned} |\Psi\rangle &= \sum_{n_a=0,1} \sum_{n_b=0,1} c_{n_a n_b} |n_a^{(a)}\rangle \otimes |n_b^{(b)}\rangle \\ &\equiv \sum_{n_a=0,1} \sum_{n_b=0,1} c_{n_a n_b} |n_a^{(a)} n_b^{(b)}\rangle \end{aligned} \quad (17)$$

where we assume two quantum states for each particle,  $|0\rangle$  and  $|1\rangle$ .

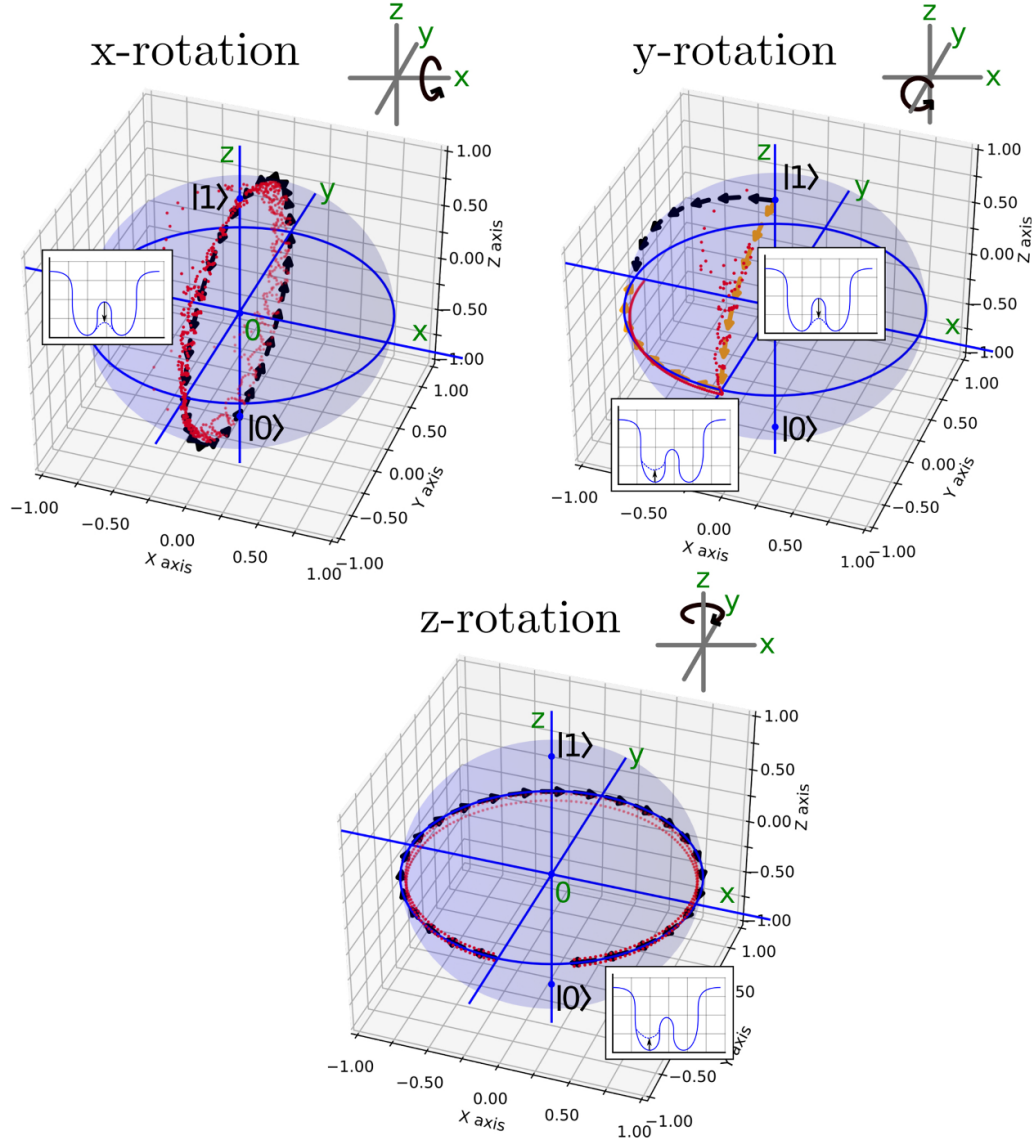


**Figure 3.** Single qubit rotation gates as simulated with a numerical method which solves the time-dependent Schrödinger equation (using the split operator method) and Lindblad formalism.

**Table 1.** Parameters used for simulations of the single-qubit rotation quantum gates.

Elementary charge, $e$	$1.602 \times 10^{-19}$	C
Effective mass, $m_e^*$	$1.08 \times 9.109 \times 10^{-31}$	kg
Length unit, $x_0$	20	nm
Energy unit, $E_0$	$\hbar^2/2m_e^*x_0^2 = 1.41 \times 10^{-23}$	J
	= 87.6	$\mu\text{eV}$
Time unit, $t_0$	$2\pi\hbar/E_0 = 47.3$	ps

To investigate the entanglement and dynamics of the system of two qubits, we will use the Von Neumann entanglement entropy (EE)  $S_N$  [33]. The density operator for non-thermal states is given by the expression:

$$\hat{\rho}_{ab} = |\Psi\rangle\langle\Psi|. \quad (18)$$

Then, the Von Neumann entanglement entropy  $S_N$  is defined as follows:

$$S_N = -\text{tr}(\hat{\rho}_a \ln \hat{\rho}_b) = -\text{tr}(\hat{\rho}_b \ln \hat{\rho}_b) \quad (19)$$

where the operators  $\hat{\rho}_a$  and  $\hat{\rho}_b$  are the reduced density operators, which can be found via the partial trace as

$$\hat{\rho}_{a(b)} = \langle 0^{b(a)} | \hat{\rho}_{ab} | 0^{b(a)} \rangle + \langle 1^{b(a)} | \hat{\rho}_{ab} | 1^{b(a)} \rangle. \quad (20)$$

Then the mutual information of the system can be defined as [36]:

$$I = S_a + S_b - S_{ab}. \quad (21)$$

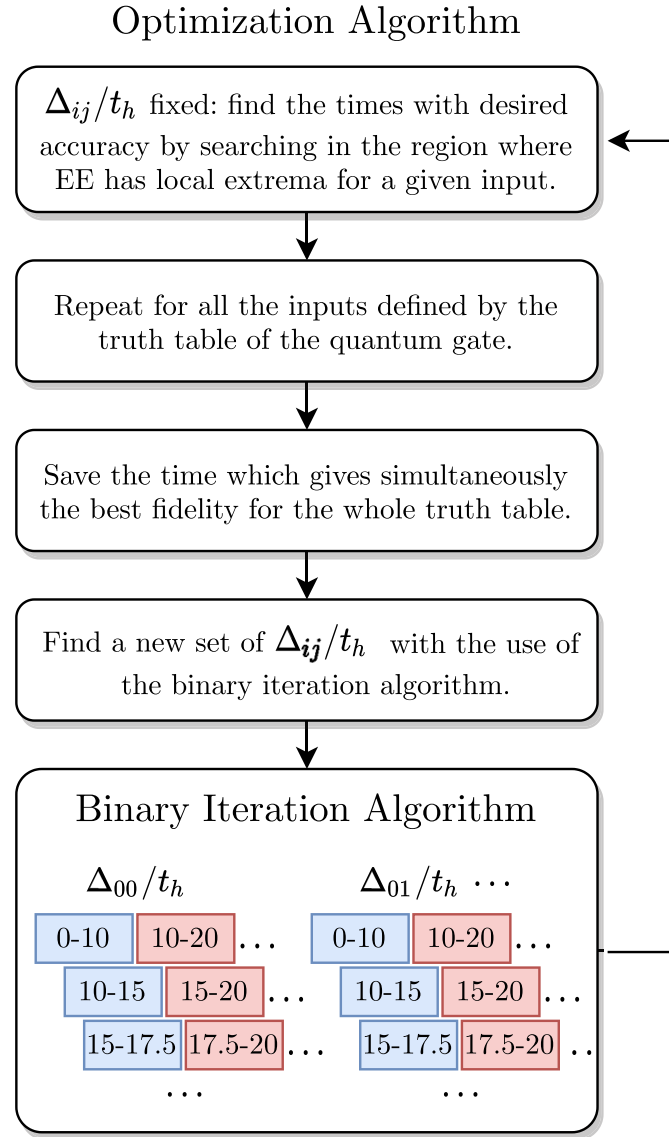


**Figure 4.** Block diagram of the optimization algorithm.

## 5.2. Optimization algorithm

After having the EE defined, we will describe in this section the optimization algorithm for the construction of two-qudit quantum gates. Initially, we will present a methodology that aims to match the amplitudes of the various quantum states. Later, we will extend this algorithm to include also non-diagonal terms. A block diagram of this is depicted in figure 4.

Based on the evolution of the quantum states and EE, we can calculate the system parameters as follows:

- For a given set of parameters  $\Delta_{ij}$  for the Hamiltonian (16), find the times at which an arbitrary threshold value of accuracy for the desired output is reached (where the desired output is defined in this case by the truth table of a specific quantum gate). This is carried out by searching in an interval around the regions where EE prohibits a local extremum.

For the given initial conditions and for the process of optimizing the SWAP gate, such an example of the evolution of various quantum states and EE is visualized in figure 5.

- Repeat this process for all the possible inputs (initial conditions) and desired outputs as determined by the truth table for a given quantum gate.
- Gather all time instances for each particular input that meet the criterion of accuracy for an arbitrary threshold value. The timing which gives the best accuracy simultaneously for all the inputs is then saved.
- Change  $\Delta_{ij}/t_{ij}$ , following a binary iteration algorithm and repeat until it converges to the desired accuracy.

**5.2.1. Binary iteration algorithm.** The binary iteration algorithm aims to optimize the  $\Delta_{ij}/t_{ij}$  parameters. In the case of two-qubit quantum gates, there are four such terms and in the case of two-qudit quantum gates, there are nine such terms



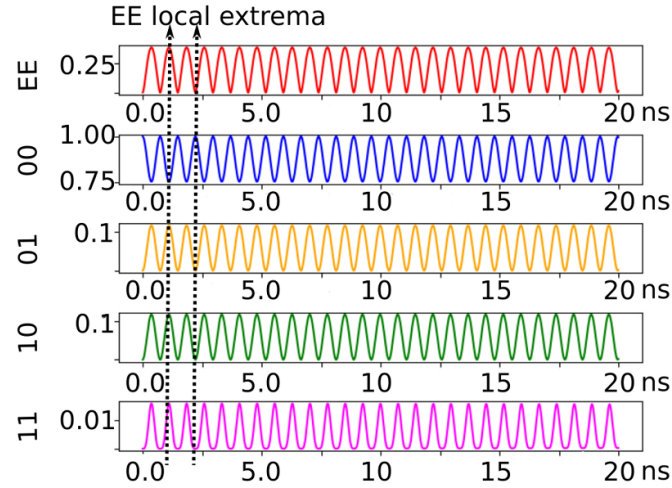


**Figure 5.** Evolution of EE and probabilities of the various quantum states for a two-qubit system. The local extrema of EE are the regions the optimization algorithm uses for finding the best timing for particular  $\Delta_{ij}$  parameters and the truth table of a quantum gate.

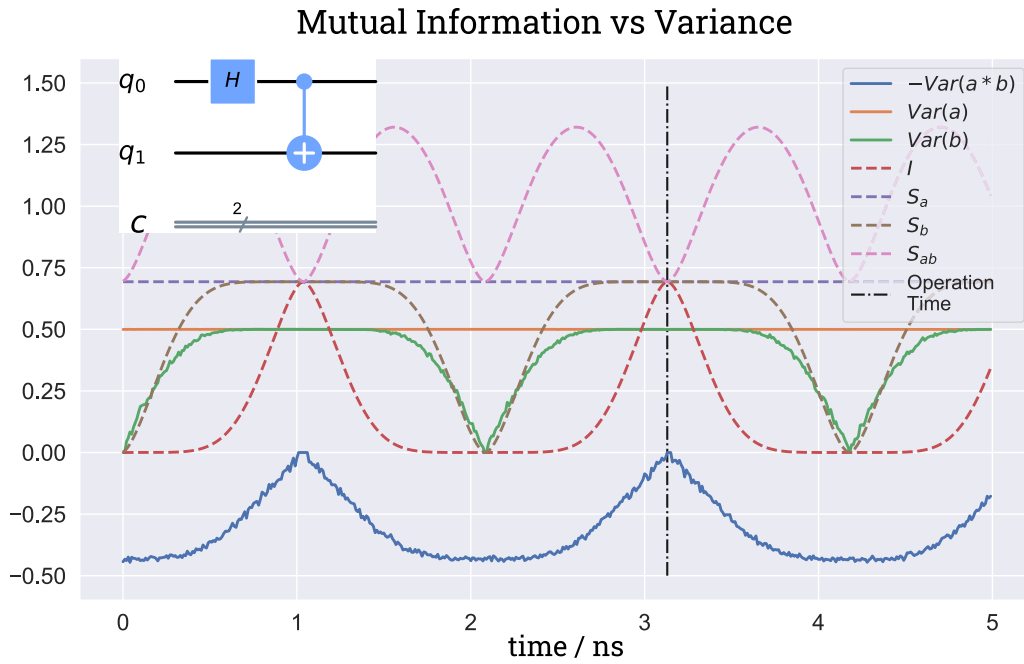


**Figure 6.** Evolution of entanglement entropy ( $S$ ), mutual information ( $I$ ), and variance ( $\text{Var}$ ), of the various quantum states and distributions of the random variables as simulated measurements at the detectors for the quantum circuit shown in the inset. The scheme can be used for the optimization of a two-qubit/qudit gate. For a maximally entangled state at the output, the EE, MI and variance are at maximum.

(the number of terms is equal to the number of diagonal terms in the Hamiltonian).

To achieve the optimization:

- We split the parameter space for each parameter  $\Delta_{ij}/t_{ij}$  into an arbitrary number of segments. An arbitrary number of points is selected for each segment.
- Then, for all the possible combinations of these selected points, we calculate the achieved fidelity of the quantum gate.
- In every instance, the timing of the quantum gate for the particular combination of parameters is calculated through the optimization procedure described above with the help of EE.
- From this process, we find in which of the segments for each parameter the best fidelity is achieved. Then, we proceed by splitting again the parameter space and repeating the process.
- Finally, after getting the best possible results from this process, we tune each parameter separately by keeping the rest parameters and timing fixed, i.e. by increasing or decreasing it with an arbitrary step resolution and measuring the

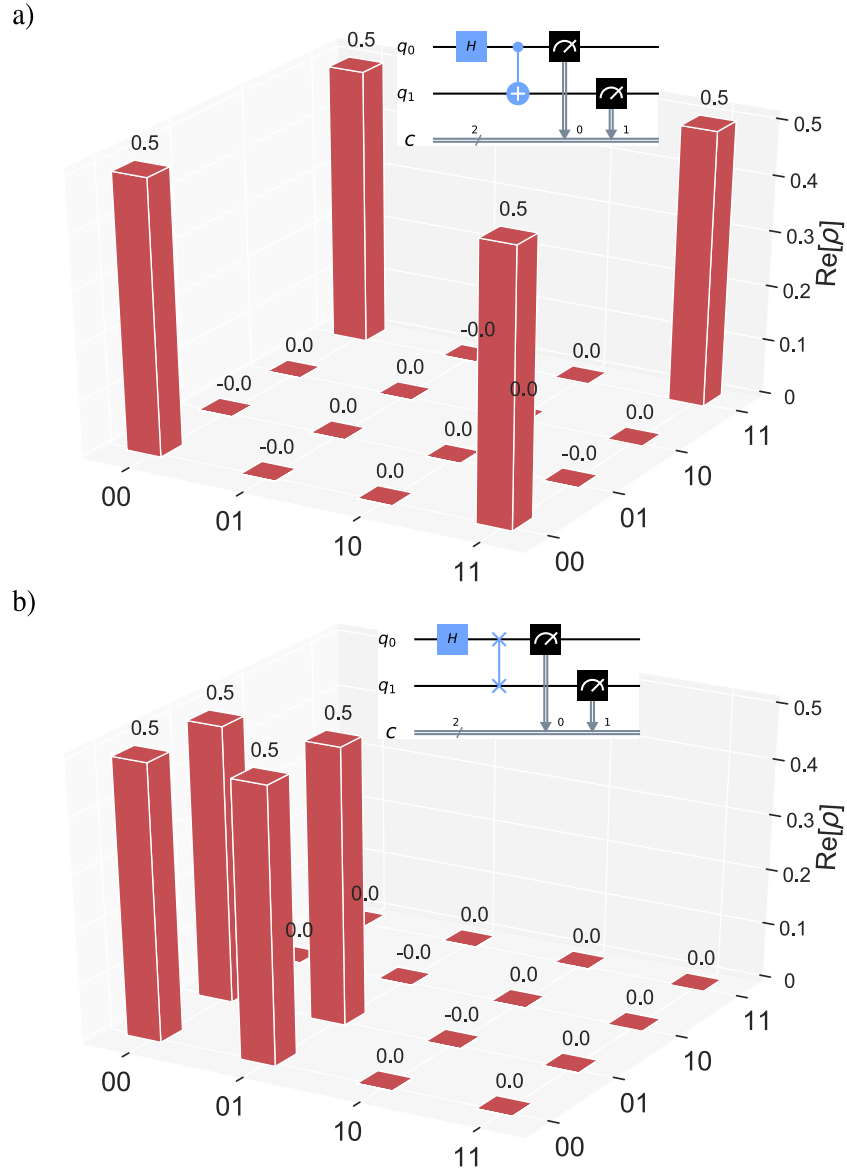


**Figure 7.** (a) Qiskit quantum circuit simulation using the developed charge qubit simulation backend. The circuit consists of two quantum registers, two classical registers, a Hadamard and a CNOT gate. (b) The circuit consists of two quantum registers, two classical registers, a Hadamard and a SWAP gate. The various states of the density matrix are visualized at the output for a given quantum circuit (inlet).

achieved fidelity. We stop increasing/decreasing each parameter when the fidelity no longer improves by the local tuning; then we move to the local tuning of the next parameter. We repeat until we achieve maximum fidelity.

### 5.3. Fitting the parameters through measurement data

The methodology presented above uses the EE to optimize the various parameters. However, EE is not a directly measurable quantity. When one desires to connect the optimization algorithm to an actual machine, one could treat it as a ‘black box’, i.e. assuming that there is no accurate information regarding the internal potential energy profile of the system and its Hamiltonian. Then, a similar strategy is still possible

to be used. Instead of trying to fit each of the entries of the truth table for a specific quantum gate, we create a more complex quantum circuit, as depicted in figure 6. We assume an ‘ideal’ Hadamard gate applied to one of the input qubit/qudit, i.e. the control qubit. The outcome is then used as an input to the CNOT gate. We can also plot the evolution of EE as defined for this two-qubit system. The task, in this case, is to find the optimized parameters for the CNOT gate. Notice that the output of this circuit is expected to be a maximally entangled state. Mutual information and EE get their maximum at specific time instances when the entanglement is maximum, as visible from figure 6.

In the actual machine, every single measurement would collapse, for each double quantum dot (i.e. qubits  $q_0, q_1$ ), to a 0

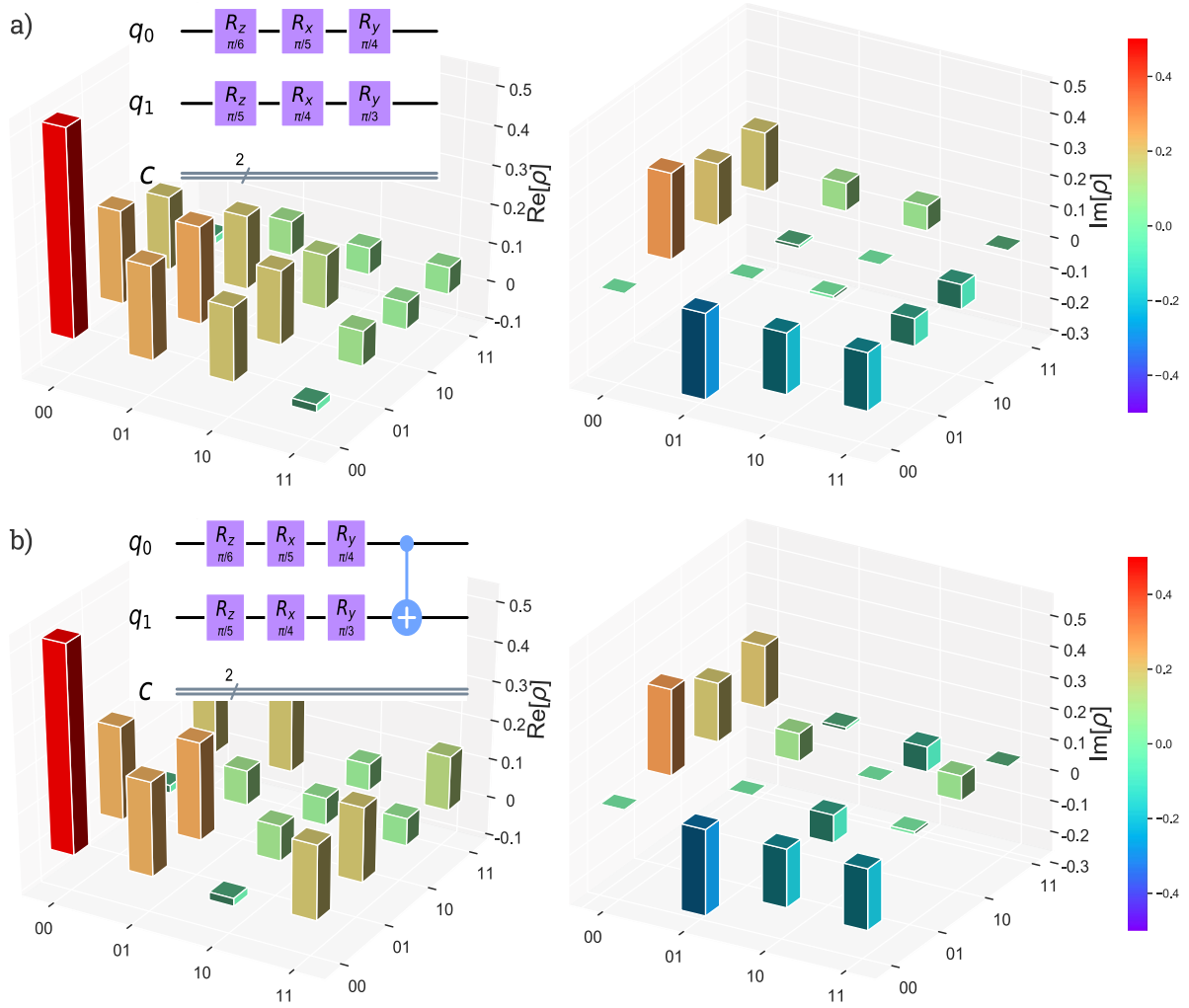


**Figure 8.** (a) Real and imaginary parts of the Qiskit quantum circuit simulation using the developed charge-qubit simulation backend (inlet). The circuit consists of two quantum registers, two classical registers, a Rotation-Z gate, a Rotation-X gate, and a Rotation-y gate. (b) Real and imaginary parts of the obtained optimized CNOT gate; the inlet depicts the quantum circuit.

or 1 logic state, depending on the position that the particle would be found. From this simulated sequence of measurements, in the same plot, we also visualize the evolution of MI and variance of the corresponding distributions of the random variables as they would be measured at the detectors. We can see that they follow a similar periodic pattern. We are interested in checking the quantum gate performance at the global peak. The result is skewed by a phase shift between different peaks. Therefore, one could either apply a correction gate, i.e. using a Z-rotation gate to compensate for this shift difference, or compare the obtained non-diagonal terms with the desired ones and choose the appropriate global peak where all conditions are met: the states are maximally entangled, the amplitudes of the quantum states match the ones of the truth table of the quantum gate and the non-diagonal terms are the ones expected. From this point of view, this suggested technique can optimize the quantum gate to fit the amplitudes of

the quantum states through measurement data, but one would require some help from simulations to also fit the non-diagonal terms.

This scheme is visualized in figure 7, where subfigure (a) demonstrates a Qiskit quantum circuit simulation using the developed charge-qubit simulation backend. The circuit consists of two quantum registers, two classical registers, a Hadamard, and a CNOT gate, whilst figure 7(b) circuit consists of two quantum registers, two classical registers, a Hadamard, and a SWAP gate. The output of the real parts of the various quantum states of the density matrix are shown for the obtained optimized parameters.

We can further extend the above idea by applying single rotation gates before applying the two-qubit/qutrit gate to both input qubits/qudits. Then, we can feed the outcome to the two-qubit/qutrit gate the parameters which we wish to optimize. This technique is useful since we can avoid optimizing

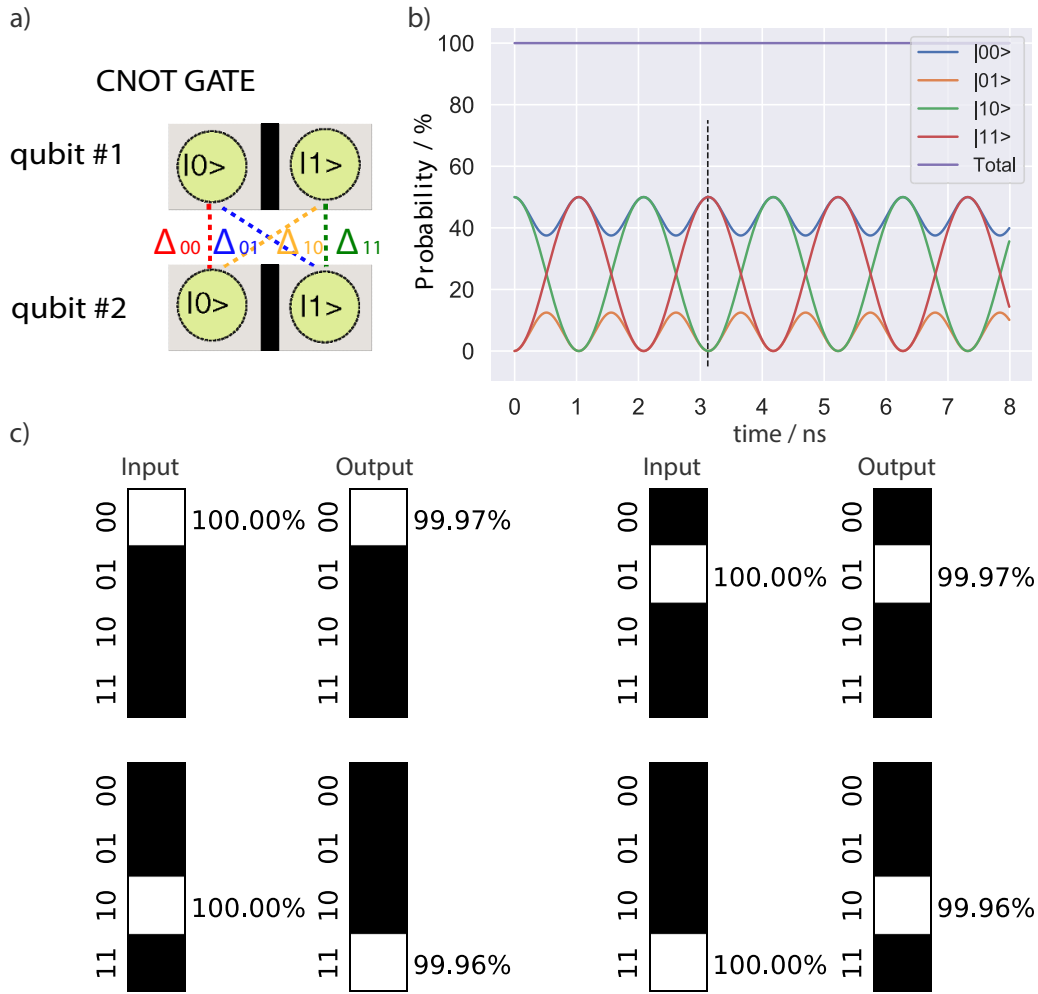


**Figure 9.** (a) Considered geometry of a two-qubit system. (b) Evolution of probabilities of the various quantum states. (c) Achieved fidelity after the optimization process for the two-qubit CNOT quantum gate for all the input/output values of the corresponding truth table.

the parameters separately for each initial condition. When one applies all possible rotations as a combination, a single optimization process is sufficient, i.e. the task is to match all the terms of the desired density matrix at the output. Then, the obtained parameters will be global; in other words, the two-qubit/qutrit quantum gates for those parameters will operate for any initial condition(s)/input(s). In this scenario, however, when the output is not a maximally entangled state, one needs to determine all parameters numerically and via simulations. The same optimization algorithm can be used, but the timing should also now be determined purely numerically, i.e. by sweeping a predefined time interval with an arbitrarily chosen time step.

This scheme is visualized in figure 8; subfigure (a) displays the real and imaginary parts of the Qiskit quantum circuit simulation using the developed charge-qubit simulation backend (see inset). The circuit consists of two quantum registers, two classical registers, a Rotation-Z gate,

a Rotation-X gate, a Rotation-y gate. The real and imaginary parts of the optimized CNOT gate are visualized in figure 8(b).

#### 5.4. Optimization taking into account decoherence

Figures 9 and 10 show what level of fidelity can be achieved after completing the proposed optimization process for the two-qubit CNOT and SWAP quantum gates taking into account the qubit decoherence. The decoherence is presented through the parameter  $\Gamma$  in equation (8). The values of the input and output of the corresponding truth tables are verified in table 2. The fidelity of the two-qubit gates as a function of  $\Gamma$  is presented in figure 11. The fidelity is expected to be worse in the case of decoherence since the evolution of the various probabilities of the quantum states is skewed. However, for a particular value of  $\Gamma$ , one can still optimize the parameters to improve the performance. In general, the shorter the

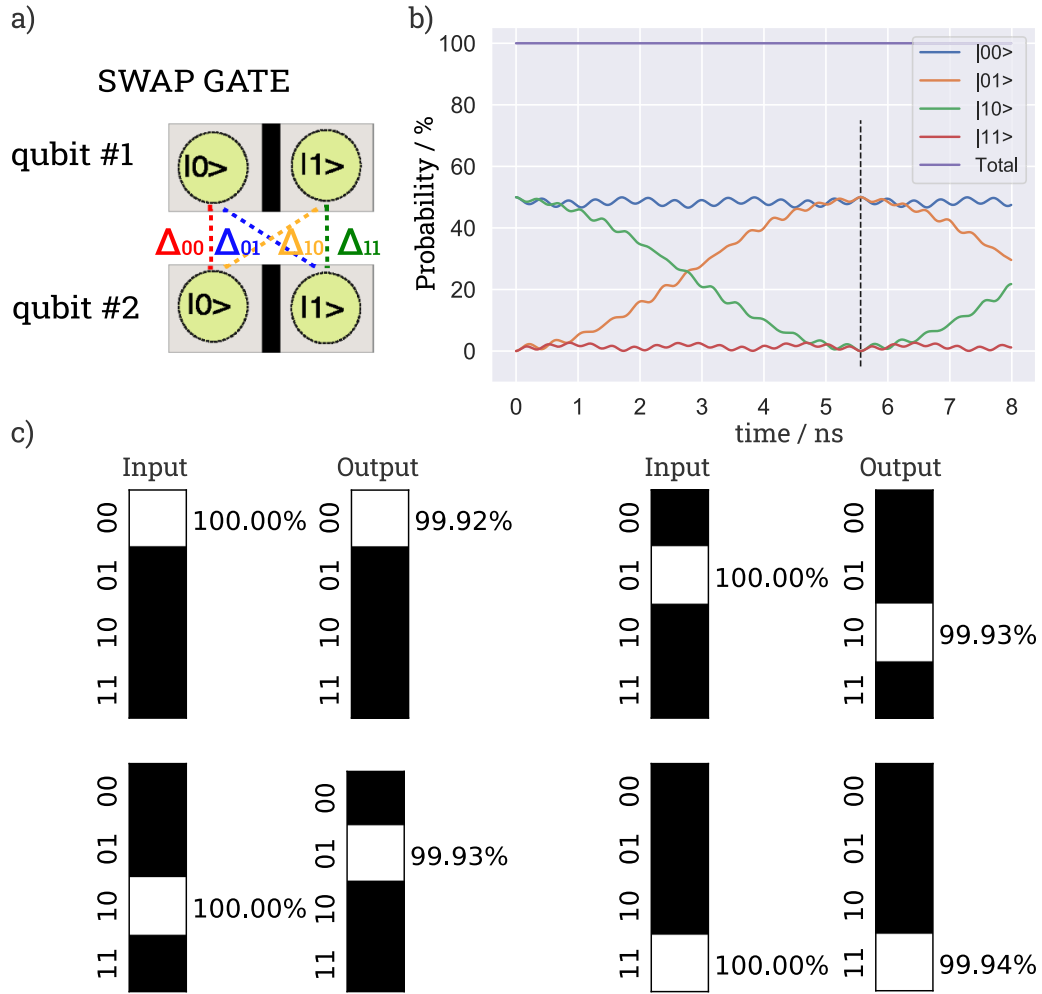


**Figure 10.** (a) Considered geometry of a two-qubit system. (b) Evolution of probabilities of the various quantum states. (c) Achieved fidelity after the optimization process for the two-qubit SWAP quantum gate for all the input/output values of the corresponding truth table.

**Table 2.** Parameters corresponding to the two-qubit gates.

Parameter	CNOT	SWAP
$\Delta_{00}$	$2.4 E_0$	$13.8 E_0$
$\Delta_{01}$	$7.6 E_0$	0
$\Delta_{10}$	$2.5 E_0$	0
$\Delta_{11}$	$2.5 E_0$	$17.2 E_0$
$t_{h,ij,\alpha}$	0	$1.5 E_0$
$t_{h,ij,\beta}$	$1.5 E_0$	$1.5 E_0$
$t_{\max}$	3.13 ns	5.56 ns

timing of the quantum gate the better the fidelity that can be achieved.

Additionally, the corresponding optimization process for the two-qubit CNOT and SWAP quantum gates is shown

in figure 12 and the parameters in table 3. The implementation of the discussed quantum gates has been implemented and integrated in Qiskit, in charge qubit simulation backend.



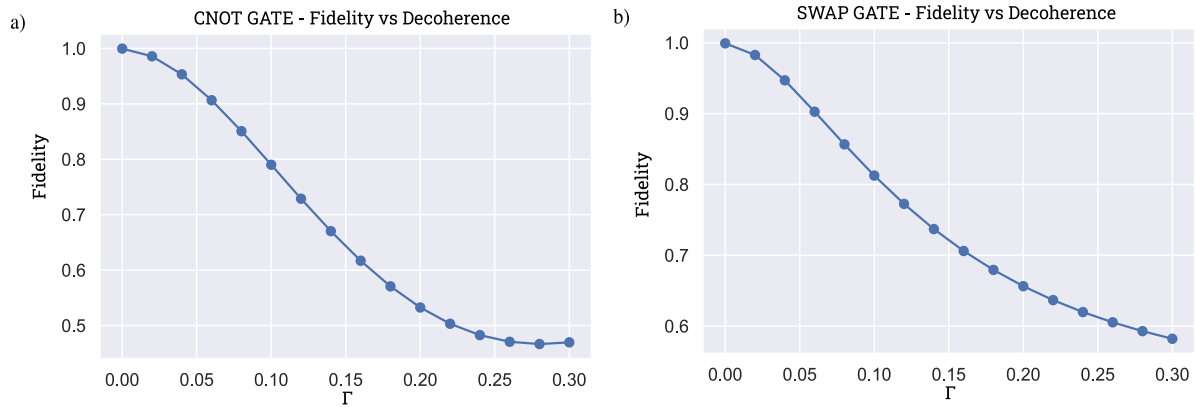


**Figure 11.** Fidelity vs decoherence for various values of parameter  $\Gamma$  for: (a) CNOT gate. (b) SWAP gate.

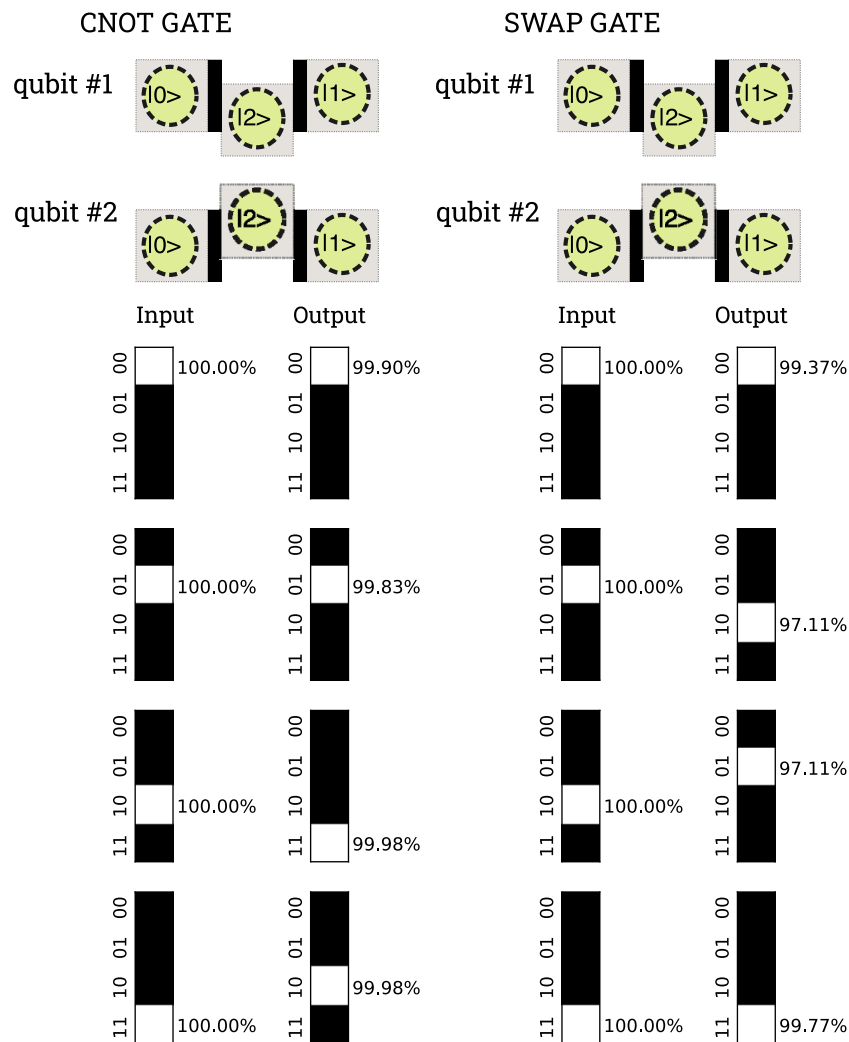


**Figure 12.** Achieved fidelity after the optimization process for the two-qubit CNOT and SWAP quantum gates for all the input/output values of the corresponding truth table.

**Table 3.** Parameters corresponding to the three-dot-qudit gates.

Parameter	CNOT	SWAP
$\Delta_{00}$	$14.0 E_0$	$10.73 E_0$
$\Delta_{01}$	$4.0 E_0$	0
$\Delta_{02}$	$13.1 E_0$	$0.05 E_0$
$\Delta_{10}$	0	0
$\Delta_{11}$	$9.0 E_0$	0
$\Delta_{12}$	0	0
$\Delta_{20}$	$5.0 E_0$	$0.03 E_0$
$\Delta_{21}$	$13.8 E_0$	0
$\Delta_{22}$	$5.0 E_0$	$18.58 E_0$
$t_{h,ij,\alpha}$	0	$1.5 E_0$
$t_{h,ij,\beta}$	$1.5 E_0$	$1.5 E_0$
$t_{\max}$	6.43 ns	16.37 ns

## 6. Conclusion

In this study, we investigated the single- and multiple-qubit/qudit quantum gates for semiconductor position-based charge qubits in FD-SOI CMOS technology. We proposed an optimization algorithm based on entanglement entropy and mutual information for the construction of two-qubit/qudit quantum gates, and we demonstrated simulation results employing quantum circuits integrated in IBM's Qiskit environment. We also suggested a methodology to connect the optimization of system parameters through simulated measurement data as it would be obtained from the system detectors with the use of mutual information (MI) and variance (Var) of the various random variables and their distributions. The optimization process applies to both qubits and qudits and can be applied to a wide range of structures/technologies.

## Acknowledgment

The authors acknowledge support through Science Foundation Ireland under Grants 14/RP/I2921 and 13/RC/2077.

## ORCID iDs

Panagiotis Giounanlis  <https://orcid.org/0000-0002-6109-5598>

Robert Bogdan Staszewski  <https://orcid.org/0000-0001-9848-1129>

## References

- [1] Nadj-Perge S, Frolov S, Bakkers E and Kouwenhoven L P 2010 Spin-orbit qubit in a semiconductor nanowire *Nature* **468** 1084–7
- [2] Jock R M *et al* 2018 A silicon metal-oxide-semiconductor electron spin-orbit qubit *Nat. Commun.* **9** 1–8
- [3] Sarma S D, Wang X and Yang S 2011 Hubbard model description of silicon spin qubits: charge stability diagram and tunnel coupling in Si double quantum dots *Phys. Rev. B* **83** 235314
- [4] Blokhina E, Giounanlis P, Mitchell A, Leipold D R and Staszewski R B 2019 CMOS position-based charge qubits: theoretical analysis of control and entanglement *IEEE Access* **8** 4182–97
- [5] Li Y-C, Chen X, Muga J and Sherman E Y 2018 Qubit gates with simultaneous transport in double quantum dots *New J. Phys.* **20** 113029
- [6] Burkard G, Loss D and DiVincenzo D P 1999 Coupled quantum dots as quantum gates *Phys. Rev. B* **59** 2070
- [7] Cayao J, Benito M and Burkard G 2020 Programable two-qubit gates in capacitively coupled flopping-mode spin qubits *Phys. Rev. B* **101** 195438
- [8] Frees A, Mehl S, Gamble J K, Friesen M and Coppersmith S 2019 Adiabatic two-qubit gates in capacitively coupled quantum dot hybrid qubits *npj Quantum Inf.* **5** 1–6
- [9] Veldhorst M *et al* 2015 A two-qubit logic gate in silicon *Nature* **526** 410–14
- [10] Shulman M D, Dial O E, Harvey S P, Bluhm H, Umansky V and Yacoby A 2012 Demonstration of entanglement of electrostatically coupled singlet-triplet qubits *Science* **336** 202–5
- [11] Sigillito A, Gullans M, Edge L, Borselli M and Petta J 2019 Coherent transfer of quantum information in a silicon double quantum dot using resonant swap gates *npj Quantum Inf.* **5** 1–7
- [12] Zajac D, Sigillito A, Russ M, Borjans F, Taylor J, Burkard G and Petta J 2017 Quantum CNOT gate for spins in silicon (arXiv:1708.03530)
- [13] Qureshi M S, Sen P, Andrews J and Sen P K 2008 All optical quantum CNOT gate in semiconductor quantum dots *IEEE J. Quantum Electron.* **45** 59–65
- [14] Yang Y-C, Coppersmith S and Friesen M 2019 Achieving high-fidelity single-qubit gates in a strongly driven charge qubit with 1/f charge noise *npj Quantum Inf.* **5** 1–6
- [15] Li H-O, Cao G, Yu G-D, Xiao M, Guo G-C, Jiang H-W and Guo G-P 2015 Conditional rotation of two strongly coupled semiconductor charge qubits *Nat. Commun.* **6** 1–9
- [16] Brif C, Chakrabarti R and Rabitz H 2010 Control of quantum phenomena: past, present and future *New J. Phys.* **12** 075008
- [17] Cheng J, Deng H and Qian X 2020 AccQOC: accelerating quantum optimal control based pulse generation (arXiv:2003.00376)
- [18] Dong D, Wu C, Chen C, Qi B, Petersen I R and Nori F 2016 Learning robust pulses for generating universal quantum gates *Sci. Rep.* **6** 36090
- [19] Daraeizadeh S, Premaratne S P and Matsuura A 2020 Designing high-fidelity multi-qubit gates for semiconductor quantum dots through deep reinforcement learning 2020 *IEEE Int. Conf. on Quantum Computing and Engineering (QCE)* (IEEE) pp 30–36
- [20] Bashir I *et al* 2020 A single-electron injection device for CMOS charge qubits implemented in 22-nm FD-SOI *IEEE Solid-State Circuits Lett.* **3** 206–9
- [21] Esmailiyan A *et al* 2020 A fully integrated DAC for CMOS position-based charge qubits with single-electron detector loopback testing *IEEE Solid-State Circuits Lett.* **3** 354–7
- [22] Fedichkin L, Yanchenko M and Valiev K 2000 Coherent charge qubits based on GaAs quantum dots with a built-in barrier *Nanotechnology* **11** 387
- [23] Gurvitz S A, Fedichkin L, Mozyrsky D and Berman G P 2003 Relaxation and the Zeno effect in qubit measurements *Phys. Rev. Lett.* **91** 066801
- [24] Fedichkin L and Fedorov A 2004 Error rate of a charge qubit coupled to an acoustic phonon reservoir *Phys. Rev. A* **69** 032311
- [25] Emary C 2008 Quantum dynamics in nonequilibrium environments *Phys. Rev. A* **78** 032105

- [26] Mathisen T and Larson J 2018 Liouvillian of the open STIRAP problem *Entropy* **20** [20](#)
- [27] Vitale S A, Wyatt P W, Checka N, Kedzierski J and Keast C L 2010 FDSOI process technology for subthreshold-operation ultralow-power electronics *Proc. IEEE* **98** [333–42](#)
- [28] Maiti C K 2017 *Introducing Technology Computer-Aided Design (TCAD): Fundamentals, Simulations and Applications* (Boca Raton, FL: CRC Press)
- [29] Shi Z *et al* 2012 Fast hybrid silicon double-quantum-dot qubit *Phys. Rev. Lett.* **108** [140503](#)
- [30] Yang S, Wang X and Sarma S D 2011 Generic Hubbard model description of semiconductor quantum-dot spin qubits *Phys. Rev. B* **83** [161301](#)
- [31] Sokolov A, Mishaghi D, Giounanlis P, Bashir I, Leipold D, Koskin E, Staszewski R B and Blokhina E 2020 Simulation methodology for electron transfer in CMOS quantum dots *Computational Science—ICCS 2020 (Lecture Notes in Computer Science)* (Springer) pp 650–63
- [32] Song H, Yang F and Wang X 2015 Condition for sudden approximation and its application in the problem of compression of an infinite well *Eur. J. Phys.* **36** [035009](#)
- [33] Giounanlis P, Blokhina E, Leipold D and Staszewski R B 2019 Photon enhanced interaction and entanglement in semiconductor position-based qubits *MDPI Appl. Sci.* **9** [4534](#)
- [34] Schaller G 2014 *Open Quantum Systems far From Equilibrium* vol 881 (Berlin: Springer)
- [35] Tabakin F 2017 Model dynamics for quantum computing *Ann. Phys.* **383** [33–78](#)
- [36] Preskill J 2016 Quantum shannon theory (arXiv:[1604.07450](#))